Designing Radiation Resistance in Materials for Fusion Energy*

S.J. Zinkle[1,2] and L.L. Snead[2]

[1]Department of Nuclear Engineering and Department of Materials Science & Engineering, University of Tennessee, Knoxville, Tennessee 37996; email: szinkle@utk.edu

[2]Oak Ridge National Laboratory, Oak Ridge, Tennessee 37831; email: sneadll@ornl.gov

Annu. Rev. Mater. Res. 2014. 44:241–67

First published online as a Review in Advance on March 26, 2014

The *Annual Review of Materials Research* is online at matsci.annualreviews.org

This article's doi:
10.1146/annurev-matsci-070813-113627

Keywords

fusion reactors, fission reactors, neutron irradiation, structural materials, displacement damage

Abstract

Proposed fusion and advanced (Generation IV) fission energy systems require high-performance materials capable of satisfactory operation up to neutron damage levels approaching 200 atomic displacements per atom with large amounts of transmutant hydrogen and helium isotopes. After a brief overview of fusion reactor concepts and radiation effects phenomena in structural and functional (nonstructural) materials, three fundamental options for designing radiation resistance are outlined: Utilize matrix phases with inherent radiation tolerance, select materials in which vacancies are immobile at the design operating temperatures, or engineer materials with high sink densities for point defect recombination. Environmental and safety considerations impose several additional restrictions on potential materials systems, but reduced-activation ferritic/martensitic steels (including thermomechanically treated and oxide dispersion–strengthened options) and silicon carbide ceramic composites emerge as robust structural materials options. Materials modeling (including computational thermodynamics) and advanced manufacturing methods are poised to exert a major impact in the next ten years.

1. INTRODUCTION

Access to reliable, environmentally sustainable, and economically competitive energy is important for worldwide economies (1). Nuclear fission energy is one of several options for clean energy; it currently provides approximately 13% of the worldwide electricity and, along with hydroelectricity, currently provides the vast majority of non-CO_2-emitting electricity (2). A variety of next-generation fission reactor concepts are currently in various stages of development (2). Nuclear fusion, presently under development worldwide, offers the potential for further enhancements in safety and has been identified by the US National Academy of Engineering as one of the top grand challenges for engineering in the twenty-first century.

1.1. Overview of Nuclear Fusion

Nuclear fusion involves the joining of two light nuclei to create a heavier (energetically more stable) nucleus, resulting in a large release of energy. Of the dozens of potential fusion reactions, the easiest in terms of confinement requirements (nuclear cross section) and ignition temperature is the fusion of the deuterium (D) and tritium (T) isotopes of H, which has a net energy release of 17.6 MeV per reaction (3, 4):

$$^{2}\mathrm{H} + {}^{3}\mathrm{H} \rightarrow {}^{3}\mathrm{He}\ (3.5\ \mathrm{MeV}) + n\ (14.1\ \mathrm{MeV}). \qquad 1.$$

Overcoming the coulombic repulsive forces of the fusing nuclei requires high kinetic energy (temperature); at these high temperatures, a neutral plasma of energetic ions and electrons is formed. For the D-T reaction, the fuel temperature must exceed $\sim 2 \times 10^8$ degrees Celsius ($\sim$20 keV kinetic energy) to achieve the fusion reaction rates appropriate for commercial energy production (3–5). Because tritium is not a naturally stable isotope, it would need to be produced via neutron reactions with Li that are accomplished within the blanket structure of the fusion reactor.

There are two complementary approaches by which to achieve the high plasma densities and temperatures needed for practical fusion energy. Magnetic fusion energy (MFE) utilizes intense ($\sim$10-T) magnetic fields for steady-state plasma confinement at moderate pressures and temperatures. For such a D-T fusion reactor, the necessary plasma density is $\sim 2 \times 10^{20}$ nuclei/m^3 (with a plasma pressure of $\sim$10 atm) at a temperature near 20 keV and an energy confinement time on the order of seconds (6). In contrast, inertial fusion energy utilizes intense laser or ion beams to produce very high particle densities (which are more than 10 orders of magnitude higher than the densities produced in magnetic fusion) (4, 6) over short time periods (tens of picoseconds) (7) in a cyclic manner yielding similar time-averaged power as does MFE. Both approaches have yielded significant advances in plasma physics (4, 5), leading to the construction of major inertial (7) and magnetic (5) fusion machines designed to explore adequately confined, hot, dense plasmas near the conditions relevant for commercial fusion energy systems.

Figure 1 provides a schematic overview of the ITER international magnetic fusion device (hereafter referred to simply as ITER) currently under construction in Cadarache, France. The D-T plasma is magnetically confined in the D-shaped toroidal region of the tokamak reactor. High heat loads and high particle and neutron fluxes will impinge on the first-wall and divertor regions surrounding the plasma; **Figure 1** shows the total neutron fluxes and the anticipated lifetime fast neutron fluences for several components. Although the blanket region beyond the first wall in ITER will serve mainly for neutron shielding (to minimize radiation doses to the vacuum vessel, magnets, and cryostat), the blankets in next-step technology demonstration (DEMO) fusion reactors will also need to breed the tritium fuel and to harness fusion energy deposited as heat by the D-T fusion neutrons.

a

ITER: lifetime fast neutron fluence (n/m^2; $E > 0.1$ MeV)	DEMO fusion power reactor: annual fast neutron fluence (n/m^2; $E > 0.1$ MeV)	Component
3.7×10^{21}	5×10^{22}	Blanket
5.1×10^{14}	7×10^{15}	Magnet
1.9×10^{21}	2.6×10^{22}	Divertor
1.1×10^{19}	1.5×10^{20}	Vacuum vessel
3.4×10^{11}	4.5×10^{12}	Cryostat

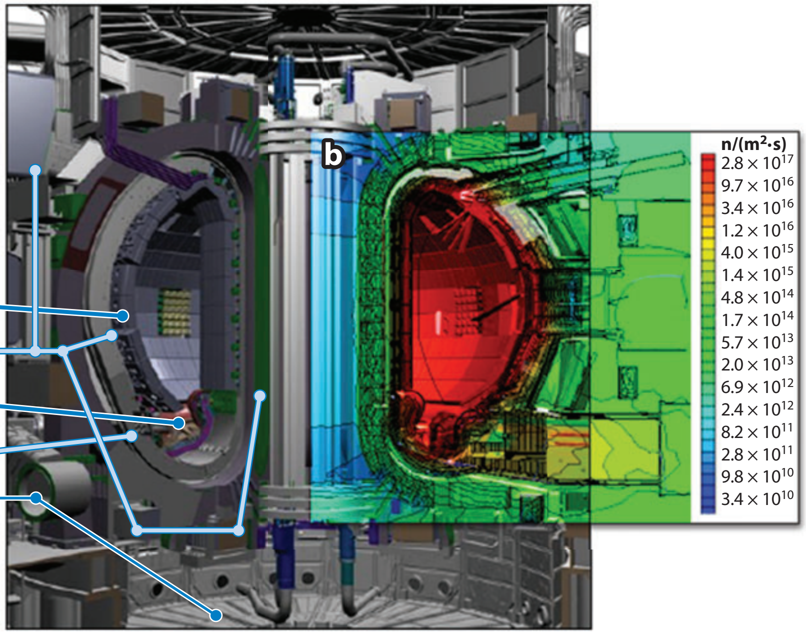

Figure 1

Overview of neutronics and cross section of the ITER tokamak. The inset figure on the right (*b*) highlights the position-dependent total neutron fluxes (based on work of R. Feder & M. Youssef). The table on the left (*a*) compares calculated fast neutron fluences for several key components in ITER and in a demonstration (DEMO) fusion reactor (based on input from M. Sawan).

A handful of blanket concepts are under consideration to harness the energy released by fusion reactions (8, 9). A wide range of coolants (water, He gas, liquid metals, molten salts) and tritium-producing blanket concepts (solid ceramics or liquid metals containing Li) are under consideration, with a correspondingly wide range of potential operating temperatures, chemical compatibility issues, and thermomechanical stresses. Most concepts utilize ferritic/martensitic steels [including oxide dispersion–strengthened (ODS) variants] as the structural material, although concepts based on SiC fiber–reinforced SiC ceramic matrix composites (SiC/SiC composites) and V alloys are also being considered (8–10). Depending on the particular blanket concept, different feasibility and operational issues arise. For example, the intense magnetic fields can profoundly influence the flow distribution (11) and corrosion (12) characteristics of liquid metal–cooled structures. In ceramic-based tritium breeding blanket concepts, difficulties with tritium extraction from ceramic pellets at low temperatures and chemical compatibility with surrounding structures at elevated temperatures narrow the potential operating temperature window (13).

1.2. Materials Challenges in Fusion Energy Systems

An important consequence of the D-T fusion reaction (Equation 1) is the generation of 14-MeV neutrons. These neutrons gradually slow down by scattering events in the materials surrounding the plasma, thereby efficiently depositing the D-T fusion energy within the first-wall and blanket region in the form of heat that is subsequently extracted to produce electricity. However, these energetic neutrons induce significant atomic displacements (vacancies and interstitials) in the

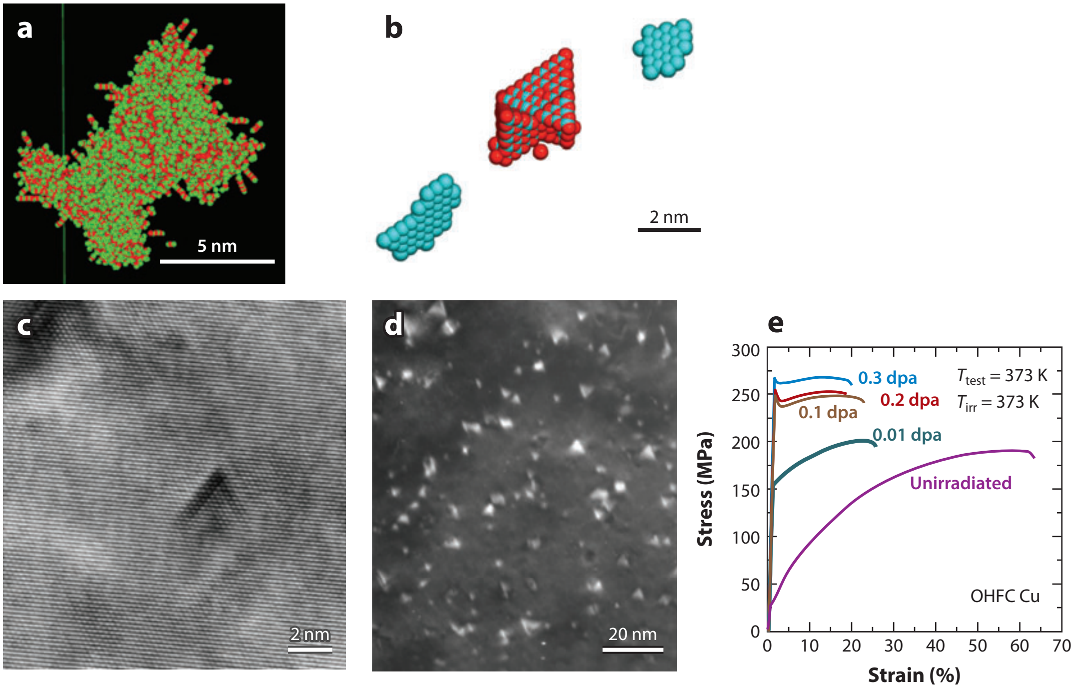

Figure 2

Example of radiation damage processes in Cu. Molecular dynamics (MD) simulation of neutron-induced 25-keV cascade damage near the transient peak displacement time (~0.25 ps) (*a*), transforming into resolvable vacancy-type stacking fault tetrahedra and interstitial-type planar dislocation loop geometries after ~30 ps (*b*). These defect clusters can be experimentally imaged (*c*,*d*) with TEM and produce hardening and loss of ductility (*e*) that become progressively more pronounced with increasing dose. The MD images (panels *a* and *b*) and the weak-beam TEM image (panel *d*) are from unpublished work by Y. Osetsky and S.J. Zinkle, respectively, and panels *c* and *e* are from References 155 and 156, respectively, with permission.

first-wall and blanket materials [as high as hundreds of displacements per atom (dpa) for anticipated 3–5-year lifetimes of the replaceable fusion structures] and generate substantial gaseous (H and He) and solid transmutation products that degrade materials properties (14–17). **Figure 2** illustrates the effect of neutron damage to Cu from the initial billiard-ball fast neutron-induced cascade of atomic displacements within the Cu lattice (**Figure 2*a***), producing highly mobile interstitials and less mobile vacancies that condense within ~10 ps to a much smaller number of defects ranging from isolated vacancies and interstitials to a variety of clustered geometries such as disk-shaped dislocation loops. For the example of **Figure 2*b***, an imperfect stacking fault tetrahedra (SFT) is predicted by molecular dynamics and can be visualized either with high-resolution transmission electron microscopy (TEM) (**Figure 2*c***) or as one of the myriad defects visualized with lower-magnification, weak-beam, dark-field TEM imaging (**Figure 2*e***). These irradiation-induced microstructural changes introduce a plethora of property degradation phenomena (summarized in Section 2), including radiation hardening and a loss of tensile ductility (**Figure 2*e***). These radiation-induced structural degradations are of concern because the technological and economic viability of fusion energy requires the structural materials to satisfactorily maintain their mechanical properties without large dimensional changes for the design lifetime of ~5 years in the presence of the extreme conditions of high fluxes of neutron radiation damage, high stress, elevated temperature, high volumetric heating, and corrosive coolants.

The economic, safety, and environmental attractiveness of fusion is linked to the development of high-performance, radiation-resistant, reduced-activation materials that minimize the waste disposition and safety burden of fusion power (14, 15). In particular, the overarching goals are production of economically competitive energy without any public evacuation for design-basis accidents or long-lived high-radioactivity waste (18). Fusion offers several potential environmental, safety, and nuclear safeguard advantages over fission power. The tritium fuel will be generated on-site, so shipping of sensitive material is eliminated after initial reactor start-up. Furthermore, because there are no radioactive products of the D-T fusion reaction, the short-term safety and long-term radioactivity burden of fusion can be minimized by utilization of the appropriate reduced-activation materials in the surrounding structure (3, 15, 19, 20). The so-called low-activation criteria are a major factor in selecting fusion materials. A handful of elements in the periodic table provide acceptable (minimal) amounts of short-term volatile and long-lived radioactive species (21, 22). However, minimizing structural damage due to fast neutron irradiation is a daunting challenge.

Whereas two of the primary elements of stainless steels (Fe and Cr) are inherently reduced activation, many of the common alloying additions such as Ni, Cu, Nb, and Mo produce undesirable radiological isotopes after exposure to D-T fusion reactor neutrons (21, 22). This situation has led fusion materials researchers to develop specially tailored (23, 24) 9–14%Cr reduced-activation ferritic/martensitic (RAFM) steels with W (replacing Mo), Ta (replacing Nb), and V (replacing Nb). Due to similarities with conventional ferritic/martensitic steels, these RAFM steels are technologically mature, satisfying many of the performance requirements for early operation of a DEMO fusion reactor. However, the operating temperature limit of RAFM steels is currently ~550°C, thus limiting the overall thermodynamic efficiency of the power plant, and as with all fusion materials, our current understanding of D-T fusion neutron radiation effects is lacking (15–17). Unfortunately, conventional austenitic steels and high-temperature Ni-based superalloys cannot be considered due to the high activation of Ni (along with concerns regarding the radiation stability of austenitic steels and superalloys).

To extend the operating temperature window for fusion reactors while maintaining low activation, several alternative materials options are being pursued. These alternatives include ODS ferritic steel, V alloys, and SiC/SiC composites. ODS steels offer the potential to increase the upper operating temperature by 100 to 200°C but are at a relatively early stage of development (16, 25–28). V alloys are a potentially attractive option for self-cooled liquid Li blankets (29) but have environmental incompatibilities with nearly all other high-temperature coolants along with radiation embrittlement concerns at operating temperatures of less than ~400°C and will require the development of robust insulating coatings (28, 30, 31). SiC/SiC composites may enable operating temperatures up to ~1,000°C and have demonstrated good radiation stability at 500–800°C during fission reactor irradiation up to 80 dpa but overall are in the early stages of incorporation into practical structural designs (32).

Considerably more challenging are the plasma-facing components of ITER and DEMO, in which materials must survive exposure to simultaneous high fluxes of heat and particles along with intense bulk neutron irradiation (33–35). As the ITER first-wall and diverter design has evolved, a number of materials have been considered: Be, carbon fiber composites, and W as surface materials (36, 37) and stainless steel and Cu alloys as substrates. High-purity Be brazed to a Cu alloy heat sink and type 316 stainless steel is currently the first-wall choice for ITER (35, 38). For the divertor, there is full coverage of W, again bonded to a Cu alloy heat sink. The selection of blanket and first-wall materials for ITER has been driven primarily by consideration of the very high particle and heat fluxes to the surfaces (along with tritium sequestration concerns and commercial availability and fabrication experience). Whereas the first-wall heat load is ~1 MW/m^2

over a pulse of several minutes, the divertor receives ~10 MW/m^2 in this time frame, and the anticipated short-term disruptions are twice that power level. ITER materials selection has also been driven by expediency, or the need to field nuclear-qualified components in the near term. Unfortunately, although these materials and components are anticipated to perform satisfactorily in the ITER environment, they are entirely unsuitable for the DEMO environment in part due to the irradiation instability of all these materials at the higher doses relevant for DEMO and violation of the low-activation criteria in the case of type 316 stainless steel and Cu. Specifically, Be suffers from a low melting temperature, severe irradiation embrittlement, and transmutation such that it is not suitable for DEMO (36, 39). W, the current leading option for beyond-ITER applications (40, 41), is notoriously difficult to manufacture and shares the very low dose embrittlement issue with Be, rendering it an essentially nonstructural material. Moreover, in a D-T fusion neutron first-wall environment, the W transmutation rate to Re and Os is ~0.25 at%/dpa (~1.4 at%/year), with unknown consequences (42).

A significant gap in the current understanding is the behavior of materials under the high neutron doses and transmutant H and He levels that are prototypical of fusion reactor first-wall and blanket structures (10, 43–45). The high neutron energy associated with the D-T fusion reaction (Equation 1) generates approximately 50- to 100-times-higher He/dpa in materials such as ferritic steels than does fission reactor irradiation. **Figure 3** summarizes current experimental He and displacement damage regimes investigated for neutron-irradiated RAFM steels compared with

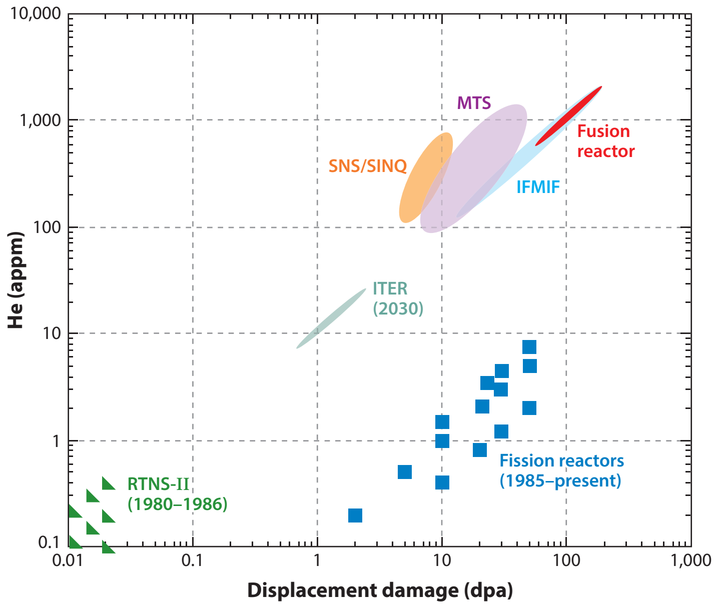

Figure 3

Summary of the RAFM steels experimental database in terms of transmutant He versus displacement damage in actual (RTNS-II, fission reactors), under construction (ITER), and proposed (SNS/SINQ, MTS, IFMIF) temperature-controlled facilities compared with the anticipated operating conditions in a demonstration fusion reactor. Abbreviations: IFMIF, proposed D-Li International Fusion Materials Irradiation Facility; MTS, proposed Materials Test Station spallation source at Los Alamos National Laboratory; RTNS, Rotating Target Neutron Source, previously at Lawrence Livermore National Laboratory; SINQ, the Swiss Spallation Source at Paul Scherrer Laboratory; SNS, Spallation Neutron Source at Oak Ridge National Laboratory.

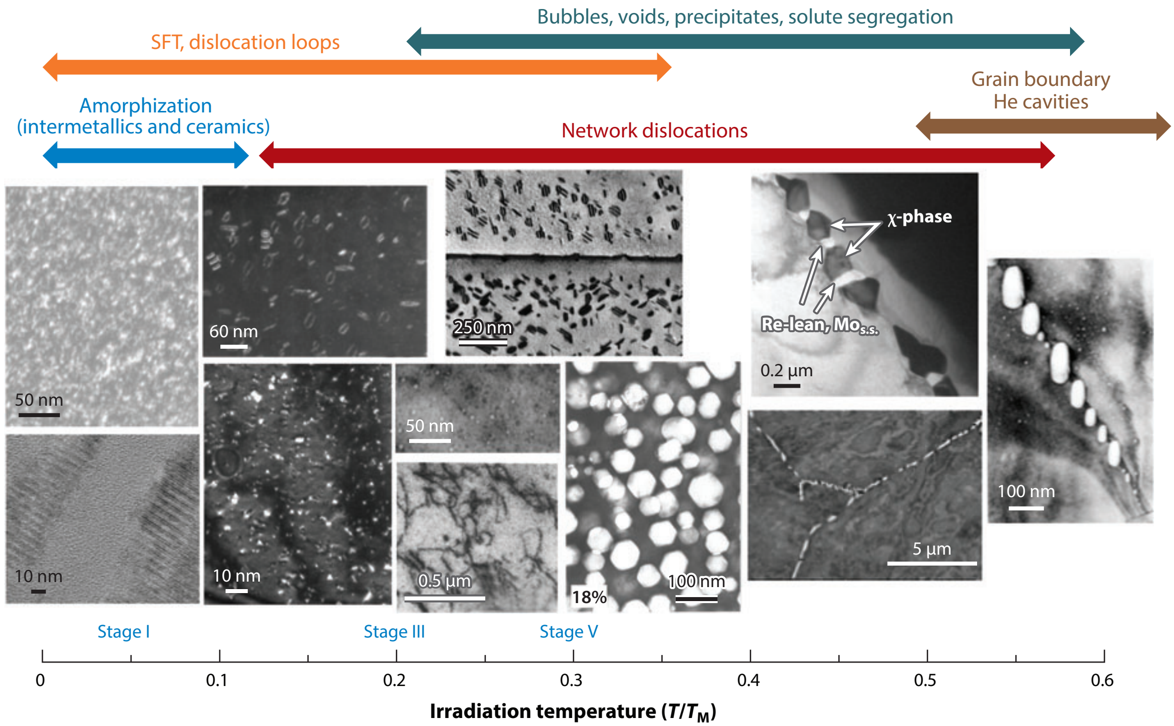

Figure 4

Examples of representative microstructures in irradiated materials as a function of irradiation temperature. The approximate onset temperatures for Stages I, III, and V of defect recovery are listed above the temperature scale, corresponding to initiation of long-range self-interstitial-atom migration, monovacancy migration, and thermal dissolution of small vacancy clusters, respectively. SFT denotes stacking fault tetrahedra.

the anticipated operating parameters to be encountered in DEMO. Although experimental data have been obtained in fission reactors for damage levels approaching DEMO-relevant doses, the level of simultaneous transmutant He generation from fission reactors is more than two orders of magnitude below that from fusion reactors. As summarized in Section 2.1, the simultaneous generation of H and He can greatly affect the microstructural evolution and accompanying property changes of irradiated materials.

2. RADIATION EFFECTS IN MATERIALS

2.1. Effects of Temperature, Dose, and Transmutant Gas

In general, the microstructural evolution in irradiated materials depends on numerous parameters, including temperature, primary knock-on atom energy, displacement dose, damage rate, crystal structure, solute additions, and transmutant elements such as H and He (46). **Figure 4** shows examples of typical temperature-dependent TEM microstructures produced in irradiated materials. Although the precise transition temperatures between different irradiated microstructural regimes are materials dependent, these transitions can be roughly approximated by using the homologous irradiation temperature (T/T_M, where T_M is the melting temperature) because the rate-controlling energies representing interstitial and vacancy migration, vacancy cluster binding or dissociation, He-vacancy complex migration, and so forth for different materials are approximately proportional to the materials melting temperature. Three particularly important transition temperatures are historically known from defect production recovery studies (47, 48) as stages I, III, and V, which correspond to the onset temperatures for long-range self-interstitial-atom migration, monovacancy migration, and thermal dissolution of small vacancy clusters, respectively. At low temperatures at which point defect migration does not occur (below recovery stage I), crystalline-to-amorphous phase transitions can be induced in many intermetallic and ceramic materials (either via direct in-cascade amorphization or via point defect accumulation processes) (46, 49). Small, diffuse point defect clusters are also created. At temperatures above stage I, distinct interstitial dislocation loops and other defect clusters are produced. At temperatures above stage III, cavity (gas-filled bubble or underpressurized void) formation can be induced, and a variety of radiation-induced solute segregation and precipitation phenomena can become pronounced. At very high temperatures, stress-assisted migration of transmutant He to grain boundaries may occur. These temperature-dependent microstructural regimes in turn induce a variety of property changes in materials.

As discussed elsewhere (17, 50, 51), there are five main radiation-induced degradation phenomena in structural materials. At low temperatures (up to stage V), rapid accumulation of thermally stable defect clusters can produce pronounced hardening and loss of macroscopic strain hardening capacity in the dose range of 0.01–1 dpa. In addition, this matrix hardening can reduce fracture toughness, and a shift in the ductile-to-brittle transition temperature to temperatures above room temperature may occur (52). At high temperatures (greater than $\sim$0.5 T_M), the combination of applied stress and transmutant He generation can induce He migration to grain boundaries and the formation of large intergranular bubbles, thereby significantly degrading the grain boundary strength (53). The low-temperature radiation-hardening and high-temperature He embrittlement phenomena typically define the allowable minimum and maximum operating temperatures, respectively, for fusion structural materials. At intermediate temperatures ($\sim$0.2–0.55 T_M), the three radiation-induced processes of void swelling (16, 46, 54, 55), phase instabilities (56, 57), and irradiation creep (54, 55) collectively define the maximum allowable operating dose for fusion structural materials for most operating scenarios. For example, volumetric expansion due to void swelling or irradiation creep is typically limited to less than $\sim$5% for structural applications, and similarly, matrix or grain boundary embrittlement due to solute segregation and precipitation cannot exceed certain levels. All five of these degradation phenomena are influenced by transmutant H and He gas generation. For example, He appears to enhance low-temperature embrittlement, possibly by nonhardening as well as by matrix-hardening mechanisms (10, 43). In addition, the enhanced cavity nucleation by He and H generally promotes void swelling and high-temperature He embrittlement, and maximum swelling is observed in some materials such as austenitic steels at fusion-relevant He/dpa values (10, 46, 58–60). However, the quantitative impact of D-T fusion-relevant H and He production is uncertain due to modeling limitations and a lack of intense fusion neutron irradiation experimental facilities (10, 43–45, 58).

In addition to the five degradation phenomena mentioned above, radiation-induced crystalline-to-amorphous phase transitions and degradation in physical properties such as thermal and electrical conductivity can be very important for some types of materials. For example, structural ceramics such as SiC/SiC composites and oxide insulators for plasma heating and diagnostic components irradiated at low temperatures at which self-interstitial atoms and/or vacancies are immobile may be susceptible to amorphization with an unacceptably high (>5%

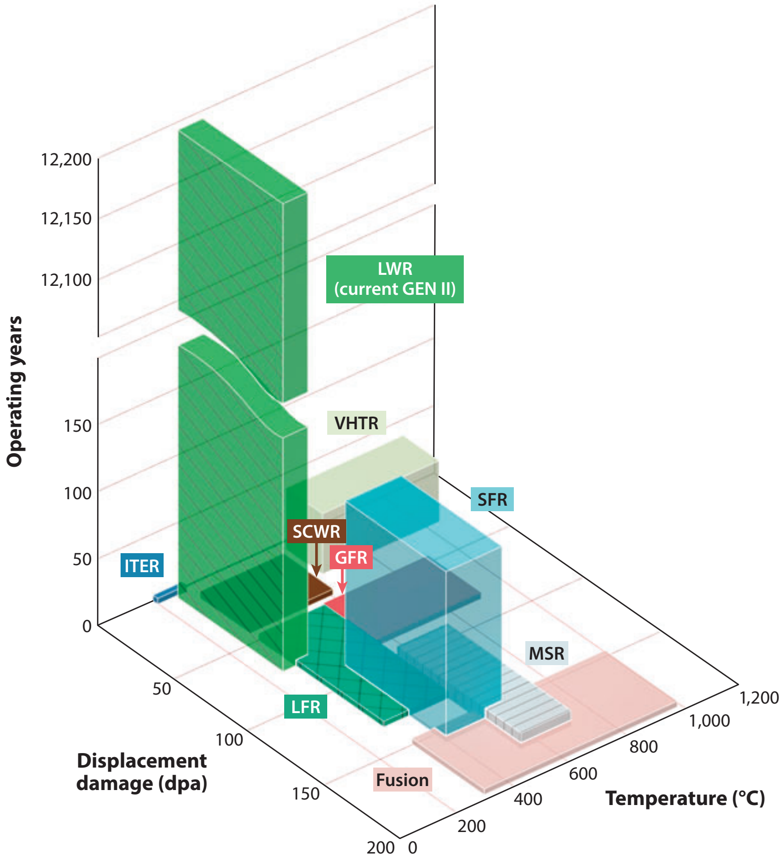

Figure 5

Overview of structural materials operational experience in a variety of civilian fission reactor systems compared with the proposed operating conditions for deuterium-tritium fusion reactors. The dose-temperature plot in Reference 17 was modified to include operational experience at or near full power. Abbreviations: GEN II, Generation II; GFR, gas-cooled fast reactor; LFR, lead-cooled fast reactor; LWR, light-water-cooled fission reactor; MSR, molten salt–cooled reactor; SCWR, supercritical water reactor; SFR, sodium-cooled fast reactor; VHTR, very high temperature reactor.

in magnitude) level of volumetric swelling (61, 62). Section 2.2 includes additional discussion of radiation-induced degradation phenomena in nonstructural materials.

There is considerable operational experience with austenitic steels and certain Ni-base alloys under commercial fission reactor irradiation conditions of ~300°C and moderate doses of up to ~50 dpa (2). In particular, more than 15,000 reactor years of civilian operating experience have been accumulated; more than 85% of this experience is associated with water-cooled reactors (63). However, the structural materials operating experience in other high-performance fission reactor irradiation environments is relatively limited. **Figure 5** compares the structural materials operating experience in current (Generation II) light-water-cooled fission reactor systems, with the operating conditions for Generation IV civilian fission reactors, ITER (under construction), and the proposed DEMO fusion reactor (2, 17, 63). Whereas light-water-cooled fission reactors have accumulated more than 12,000 reactor years at or near full power, the operating temperatures and displacement damage doses for structural materials in these reactors are relatively low. The practical operational experience with structural materials in higher-temperature, high-dose reactors is limited to approximately 140 years at or near full power in Na-cooled fast reactors (out of ~400 years of total reactor operation, including maintenance and other factors), approximately 50 full power years in very high temperature gas-cooled reactors (with low to moderate displacement damage), and approximately 1.5 full power years in molten salt reactors. As a consequence, there is limited practical experience on structural materials at the high temperatures and displacement doses anticipated for fusion.

2.2. Radiation Effects in Nonstructural Materials

The nonstructural materials of fusion power reactors will be required to reliably maintain numerous specific optical and thermophysical properties while operating over a wide range of temperatures. Applications include thermal and electrical insulators, diagnostics sensors, windows, plasma heating feedthroughs and cabling, and the constituents of superconducting magnets (64–66). In comparison with the microstructural and mechanical property performance of nuclear structural alloys, nonstructural components are typically more prone to irradiation degradation of key physical properties. For example, thermal, electrical, and optical properties may be dramatically affected by point defect production and transmutation that occurs upon neutron irradiation, even for doses of <1 dpa (66). Moreover, the materials most appropriate for many specialty applications operate at a relatively low fraction of their homologous temperature, limiting defect mobility and the ability to thermally recover radiation damage. An additional challenge is that many nonstructural materials possess covalent or ionic bonding, adding a new level of constraint to the as-irradiated microstructure. Whereas metals are essentially unaffected by ionizing radiation, glasses and some ceramic materials undergo significant volumetric, optical, and thermophysical property changes directly from absorbed gamma irradiation (67).

The required radiation hardnesses (lifetimes) of functional and engineering materials in fusion and nuclear power systems span orders of magnitude and pose serious limitations to both near-term systems such as ITER and future fusion power systems such as DEMO. Particularly radiation-sensitive materials include the glass of fiber-optic sensors (unacceptable transmission loss by $\sim10^{21}$ n/m^2) (68), the organic insulation for superconductors (loss of strength by $\sim2 \times 10^{22}$ n/m^2), thermally insulating ceramics and the superconducting materials used for magnets (pronounced degradation by $\sim10^{23}$ n/m^2), the sapphire used for optical windows (50% darkening by 5×10^{23} n/m^2) (68), and the dielectric materials used for mirrors (degradation above 10^{25} n/m^2) (69). As **Figure 1** shows, these neutron fluences are similar to the lifetime ITER fluence, but the fluences correspond to only weeks or months of service at DEMO-relevant flux levels. Although some components could be replaced as part of routine maintenance, frequent replacement of numerous nonstructural materials would be economically untenable for fusion energy. In some cases (e.g., in the case of magnets), a combination of shielding and improvements in constituent materials (e.g., better organic insulation or use of inorganic insulation) may be possible. These relatively radiation-sensitive materials and components are in stark contrast to structural materials that can generally survive to much higher neutron doses. For example, the fracture toughness of RAFM steel becomes compromised by $\sim10^{26}$ n/m^2 at ITER-relevant (<300°C) temperatures and at higher doses for anticipated DEMO (>300°C) operating temperatures (10). A similar limitation relates to irradiation-induced swelling in RAFM, in which 5% swelling is anticipated to develop after $\sim10^{27}$ n/m^2. Alumina, which is utilized in diagnostic or insulator applications, would exhibit similar levels of swelling at an order-of-magnitude-less neutron dose. For the glass used in fiber optics, a further four-order reduction in dose to achieve comparable 5% volumetric swelling is observed (70).

3. APPROACHES FOR ENHANCED RADIATION TOLERANCE IN MATERIALS

A wide variety of different approaches for developing radiation-resistant materials have been proposed and tested over the past 50 years. For example, amorphization (loss of long-range crystalline lattice structure) is perhaps the most drastic irradiation-induced change. In certain cases, crystallographic structures exhibit superior tolerance to radiation-induced amorphization that is specifically linked to ease of cation disordering (71). Similarly, high-dose radiation effects research on metals (72) initially suggested that high dislocation densities associated with cold working could delay the onset of void swelling (by providing numerous sites for the absorption of migrating point defects), but subsequent research determined that the dislocation densities in cold-worked materials generally relax under prolonged irradiation and approach values comparable to those of irradiated annealed materials after only a few dpa (73, 74). Solute additions that result in the enhancement in vacancy-solute diffusivity (16, 75, 76) or, more importantly, in the creation of a high density of matrix precipitates (16, 77, 78) also suppress void swelling and other radiation-induced microstructural changes. As discussed in this section, three general strategies can be employed to increase radiation tolerance in materials: radiation-resistant matrix phases, immobilized point defects, and engineered high-sink-strength microstructures.

3.1. Radiation-Resistant Matrix Phases

Early fundamental research on radiation effects in metals experimentally examined a wide range of atomic mass and crystal structures to explore whether certain phases might exhibit inherently superior resistance to defect accumulation (48, 79–82). More recently, molecular dynamics simulations (83) and density functional theory models (84) have provided valuable insight into defect production, migration, and clustering processes in a variety of materials. In general, metals based on face-centered-cubic (FCC) crystal structures exhibit slightly higher residual defect production efficiency than do body-centered-cubic (BCC) and hexagonal-close-packed (HCP) crystal systems (79, 80, 83). Anisotropic growth in irradiated HCP materials (which can induce microcracking and other undesirable phenomena) generally excludes HCP materials from consideration for nuclear structural applications.

Of potentially greater importance are the lower overall fraction of relatively large (TEM-visible) defect clusters and the more finely dispersed distribution of defect clusters in BCC compared with such distribution in FCC crystal systems produced directly within energetic displacement cascades (51, 82, 83). This fine dispersion of primary defects can lead to more efficient defect recombination during subsequent microstructural evolution. **Figure 6** compares the defect clusters visible by TEM in austenite (FCC) and ferrite (BCC) regions of a dual-phase steel following low-temperature neutron irradiation. The visible defect density in the FCC regions was much higher than in the BCC phase, and the resulting retained defect concentration in the dislocation loops after 0.065 dpa was approximately 30 times higher in the FCC phase.

A similar dramatic difference in defect accumulation is observed in FCC and BCC steels irradiated at higher temperatures at which void swelling occurs. **Figure 7** compares the void-swelling behavior of type 304L austenitic (FCC) stainless steel and 9–12%Cr ferritic/martensitic (BCC) steels following fast fission reactor neutron irradiation at 400–550°C (2). The observed swelling rate per dpa is approximately 50 times higher for the 304L stainless steel than for the 9–12%Cr ferritic/martensitic steels over the investigated damage levels. At higher damage levels, the steady-state swelling rates for ferritic/martensitic steels remain approximately a factor of five lower than in austenitic steels (54).

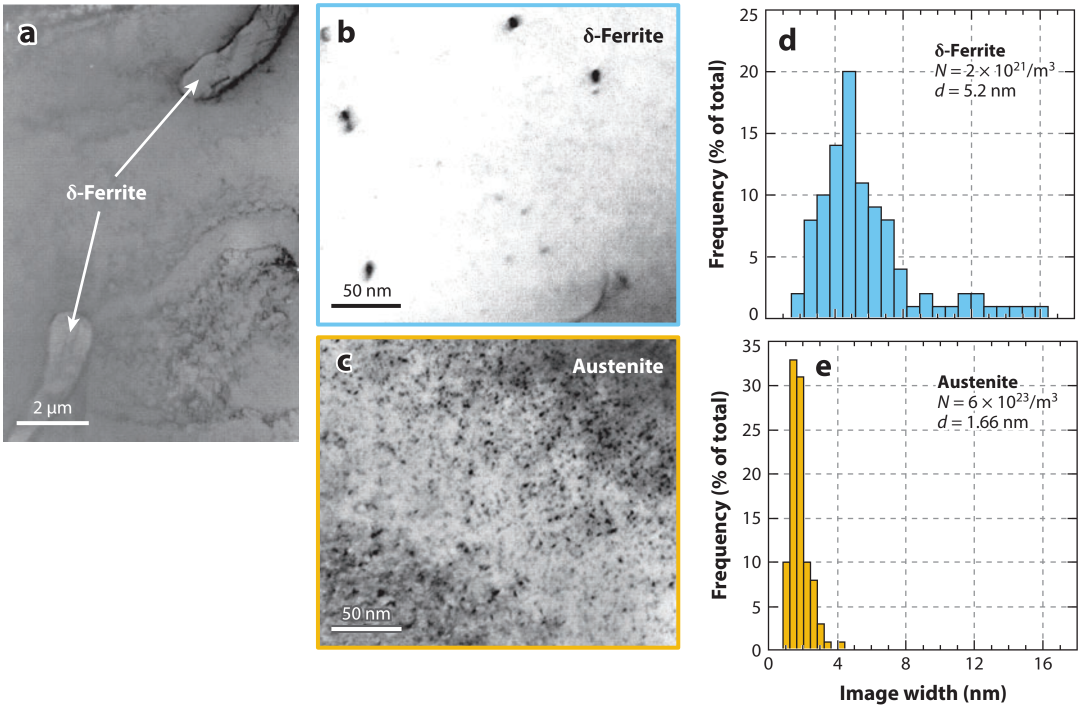

Figure 6

Comparison of visible defect cluster accumulation in body-centered-cubic (BCC) versus face-centered-cubic (FCC) regions of a type 308 stainless steel weldment after fission neutron irradiation at 120°C to 0.065 displacements per atom (dpa). (*a*) General microstructure showing BCC δ-ferrite stringers in an FCC (austenite) matrix. (*b*,*c*) Defect clusters in (*b*) δ-ferrite and (*c*) austenite regions. (*d*,*e*) The size distributions of dislocation loops in (*d*) δ-ferrite and (*e*) austenite regions. From S.J. Zinkle & R.L. Sindelar, unpublished research.

The physical mechanism(s) responsible for the generally superior radiation resistance of BCC materials is not fully understood. Possible contributing mechanisms include reduced in-cascade production of sessile point defect clusters [and overall finer dispersion of defect clusters produced within energetic displacement cascades (51, 82, 83)], lower dislocation bias (i.e., the preferential absorption of interstitials at dislocations compared with vacancies) (85), and higher self-diffusion coefficients (76). The production of finely dispersed mobile point defects and defect clusters within energetic displacement cascades promotes enhanced defect recombination compared with recombination in cases in which the defects are initially bifurcated into relatively large self-grouped vacancy and interstitial clusters; that is, on the basis of random-walk diffusion principles, the probability of vacancy-interstitial recombination events is reduced if the defects are contained in a few relatively large, low-mobility clusters as opposed to many relatively small, high-diffusivity clusters or isolated point defects. Due to significantly smaller point defect relaxation volumes (85) and the higher proportion of screw dislocations versus edge dislocations (16) in most BCC versus FCC metals, the biased absorption of self-interstitial atoms at dislocations is significantly lower in BCC metals, and vacancy accumulation is therefore suppressed due to a lack of vacancy supersaturation. The generally higher self-diffusion coefficients in BCC metals (at a given T/T_M) also enhance self-recovery diffusion mechanisms and thereby suppress radiation damage accumulation.

Although the void-swelling resistance of BCC metals is generally superior to that of FCC metals, this behavior is not universal. For example, very high void swelling (>90% after 34 dpa)

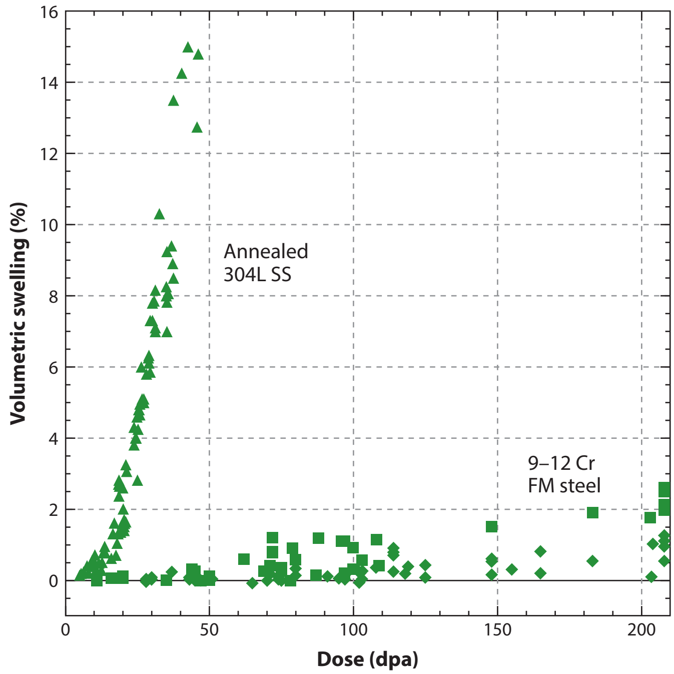

Figure 7

Comparison of void swelling in neutron-irradiated type 304L austenitic stainless steel (304L SS) and 9–12%Cr ferritic/martensitic steel (9–12 Cr FM steel) at 400–550°C.

has been observed in neutron-irradiated V-5%Fe, whereas most other V alloys exhibit very low radiation-induced void swelling (86). The high swelling in V-5%Fe has been attributed to an unusual preferential absorption of the undersized Fe solute atoms by dislocations in this alloy (87).

Several other materials systems beyond BCC alloys offer the (as-yet-unproven) potential for enhanced radiation resistance. High-entropy alloys (88) composed of approximately equimolar concentrations of multiple principal elements can possess configurational entropies that exceed the entropy changes associated with melting. Modification of the point defect recombination processes (e.g., increased point defect recombination radius) by such high configurational entropy could result in radiation resistance different from that of conventional alloys based on one primary solvent element. A recent scoping study (89) found that the solute segregation and radiation defect accumulation behavior of an ion-irradiated, high-entropy, single-phase FCC Fe-Mn-Ni-Cr alloy was indeed significantly different from the behavior of a conventional solid-solution FCC Fe-Cr-Ni or Fe-Cr-Mn alloy. In particular, pronounced Cr enrichment (rather than the depletion observed in conventional alloys) occurred at grain boundaries in the high-entropy alloy irradiated at 500°C, and void formation was not detected up to 10 dpa. Although the overall irradiation stability of the examined high-entropy alloy was not suitable due to Cr grain boundary segregation, the dramatically different solute segregation and defect clustering (void and dislocation loop) behavior of the high-entropy alloy compared with the behavior of the conventional alloys merits further study. As another example, certain ceramic crystallographic structures such as fluorites exhibit superior tolerance to radiation-induced amorphization, as discussed in the beginning of Section 3 (71, 90). This superior tolerance has been attributed to the intrinsic ability of this crystal structure to accommodate lattice disorder. Amorphous materials such as bulk metallic glasses (91) are another potential radiation-resistant materials system. Due to the lack of crystalline structure, Frenkel (vacancy-interstitial) defects are not created in glasses by energetic irradiation, although a variety of molecular defect aggregates can be produced. Whereas early radiation studies on relatively simple amorphous materials such as silica glass (92) and model nuclear waste form glasses (93) found significant radiation-induced dimensional changes, several glass compositions with good dimensional stability during prolonged irradiation have been identified (93).

3.2. Immobile Vacancies and/or Interstitials

An alternative approach to selecting radiation-resistant materials is to choose materials for which one or both of the radiation-induced point defects (interstitials and vacancies) are immobile at the anticipated operating temperatures. This choice provides the potential to directly introduce point defect recombination centers as a result of the neutron irradiation. If none of the created point defects are mobile, then the defect concentration linearly increases with dose until it approaches a saturation concentration generally determined by the spontaneous recombination distance for vacancy-interstitial pairs or by impingement of displacement cascades on preexisting defect clusters (94–96). In practice, this saturation concentration is reached after ~0.1 to 1 dpa, with typical values of ~0.1 at% for metals and ~1 to 5 at% for ceramics; the higher atomic concentrations in ceramics are due to higher point defect recombination barriers compared with those in metals (97). **Figure 8** compares the temperature-dependent saturation volumetric swelling in several materials at temperatures and doses above the critical temperature for amorphization and below the onset of void swelling, i.e., within the point defect swelling regime in which interstitials are mobile and vacancies are sessile (98–100). The point defect swelling for all materials decreases with

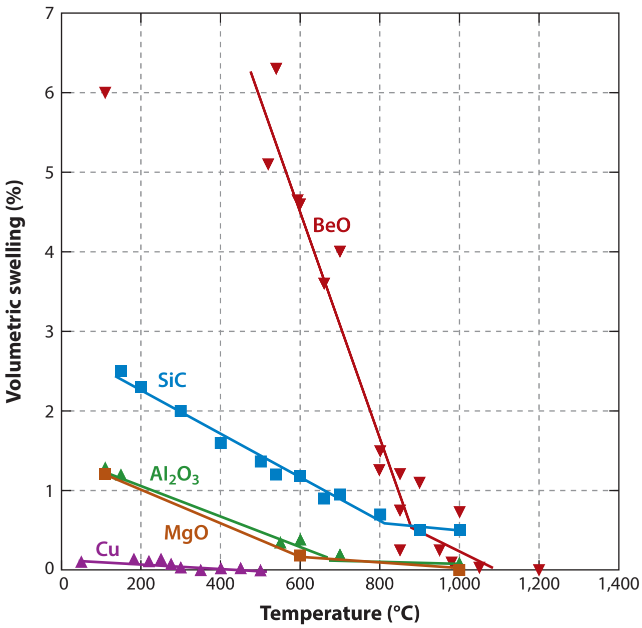

Figure 8

Comparison of point defect swelling behavior in irradiated metals and ceramics. The Cu lattice expansion data are taken from X-ray measurements of specimens irradiated in the ORR fission test reactor. From S.J. Zinkle & B.N. Singh, unpublished research.

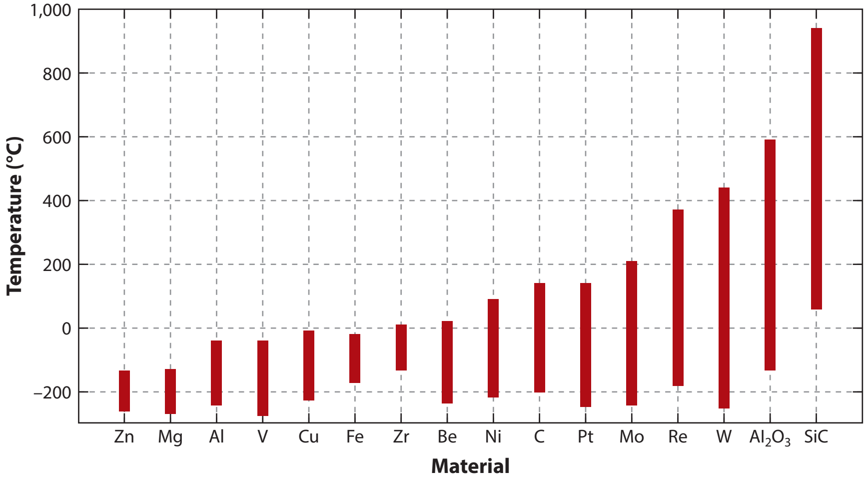

Figure 9

Temperature intervals associated with onset of interstitial migration (defect recovery above Stage I) and prior to vacancy migration (below Stage III) in selected materials.

increasing temperature due to thermal-activated migration and dissolution of small defect clusters. The point defect swelling of BeO at low temperatures is unacceptably high and anisotropic (due to the HCP structure), leading to pronounced microcracking and loss of strength. Microcracking and loss of strength are also observed in coarse-grained Al_2O_3 (but not in fine-grained Al_2O_3) due to anisotropic swelling within individual grains of this HCP material (101). Microcracking has not been observed in irradiated cubic SiC or MgO ceramics, and the swelling at a given temperature remains constant for doses from more than ~0.1 dpa to at least 40 dpa in neutron-irradiated SiC (32, 102). The point defect swelling values in metals such as Cu and Ni [maximum saturations $\Delta V/V \sim 0.1$–0.2% (95, 96)] are much lower than in ceramics, which implies smaller point defect recombination radii and/or reduced energy barriers for point defect recombination for these metals.

For intermetallics and ceramic materials, there is a potential for crystalline-to-amorphous phase transitions (with accompanying undesirable large volumetric changes) if both interstitials and vacancies are immobile (46). For example, SiC experiences a volumetric expansion of ~11% due to amorphization when neutron irradiated at temperatures of less than ~100°C (103). Therefore, for practical application of the immobile point defect concept, the irradiation temperature during operation should be above recovery stage I (to avoid amorphization in ceramics and intermetallics) and below stage III (to avoid the void-swelling regime). **Figure 9** summarizes the temperature range above stage I and below stage III for selected materials on the basis of point defect mobility data summarized in Reference 46 and graphite data summarized in Reference 104. For most metallic elements, the onset for vacancy motion occurs at too low temperatures for practical application of this radiation-resistant mechanism in nuclear energy systems; Re and W are the only possible metallic candidates, even for relatively low temperature water-cooled reactor concepts. Other potential materials systems such as Al_2O_3 exhibit susceptibility to microcracking due to their anisotropic crystal structures. However, SiC/SiC composites emerge as an attractive structural materials candidate for nuclear energy systems due to the wide potential operating window of ~200–950°C. The very high density of small interstitial clusters and isolated or clustered vacancies (~$10^{29}/m^3$) provides numerous sites for point defect recombination. By using the sink strength estimates discussed in Section 3.3, a very high sink strength density of $\sim 10^{18}/m^2$ is calculated. SiC does not exhibit good radiation resistance when irradiated at temperatures greater than the onset for vacancy migration; significant void swelling begins to occur in SiC at irradiation temperatures greater than 1,000°C due to the onset of Si vacancy mobility and becomes pronounced above 1,300–1,400°C due to C vacancies becoming mobile (105).

3.3. Engineered High Sink Strength

The predominant effort worldwide for designing radiation-resistant materials since the early 1970s has been based on the introduction of a high density of point defect recombination centers (generally referred to as point defect sinks). This activity has been motivated by kinetic rate theory models (55, 106, 107) that have shown a pronounced reduction in point defect supersaturation values and related phenomena such as void swelling and radiation-induced solute segregation when high sink strengths are present. Numerous experimental studies have verified the importance of high concentrations of dislocations (72, 108, 109) and finely dispersed precipitates (74, 77, 78, 110, 111) in void-swelling suppression.

The quantitative point defect capture effectiveness of various microstructural features has been analyzed by using kinetic rate theory. The sink strength of cavities of radius r_C and number density N_C is given by (55)

$$S_C = 4\pi r_C N_C (1 + S^{1/2} r_C) Z_C, \qquad 2.$$

where S is the cumulative sink strength of all sinks and Z_C is the cavity sink capture efficiency of order unity. A similar expression can be used for spherical precipitates or dispersoids. The sink strength of grain boundaries is given by $S_{gb} = 60/d^2$ when $S^{1/2}d \ll 1$ and by $S_{gb} = 6S^{1/2}/d$ when $S^{1/2}d \gg 1$, where d is the grain diameter. The sink strength for dislocations is $S_d = Z_d \rho_d$, where Z_d is the dislocation capture efficiency of order unity.

Figure 10 summarizes the effect of initial sink strength on the radiation-hardening behavior of several types of ferritic/martensitic steels (including ODS steels) following fission neutron irradiation near 300°C (10, 112–114). There is relatively little influence on radiation hardening for sink strengths of up to $\sim 10^{16}/m^2$, but there is a clear trend for reduced radiation hardening at very high sink strengths ($>10^{16}/m^2$). A similar trend for reduced radiation degradation at very high sink strengths has been observed in the fracture toughness of fission neutron–irradiated ODS and ferritic/martensitic steels after ~1.5 dpa at 300°C (112). Similarly, at high temperatures, high densities of sinks such as precipitates can efficiently trap He and thereby suppress high-temperature He embrittlement (16, 53, 115–117). Therefore, high-sink-strength modifications have the potential to beneficially suppress low-temperature radiation hardening and high-temperature He embrittlement and thereby expand the operating temperature window for structural materials in nuclear energy systems.

At intermediate temperatures, high sink strengths also beneficially suppress void swelling (16, 74, 77, 78, 110, 111) and thereby enable higher lifetime doses. **Figure 11** summarizes a few examples of the effect of overall sink strength (precipitates, dislocation loops, network dislocations, and cavities) on void swelling of Fe-Cr-Ni austenitic alloys irradiated near the peak swelling temperature (118–121). These results suggest that sink strengths greater than $\sim 10^{15}/m^2$ (typically created by the introduction of a high density of fine precipitates) effectively suppress void swelling. Analysis of the critical radius for conversion of He-filled bubbles to bias-driven voids in high-dose irradiation studies on a variety of austenitic and ferritic/martensitic steels has found that sink strengths greater than $\sim 10^{16}/m^2$ are generally needed to provide superior void-swelling resistance (122, 123). Among the structural alloys currently under investigation, finely dispersed nanoclusters

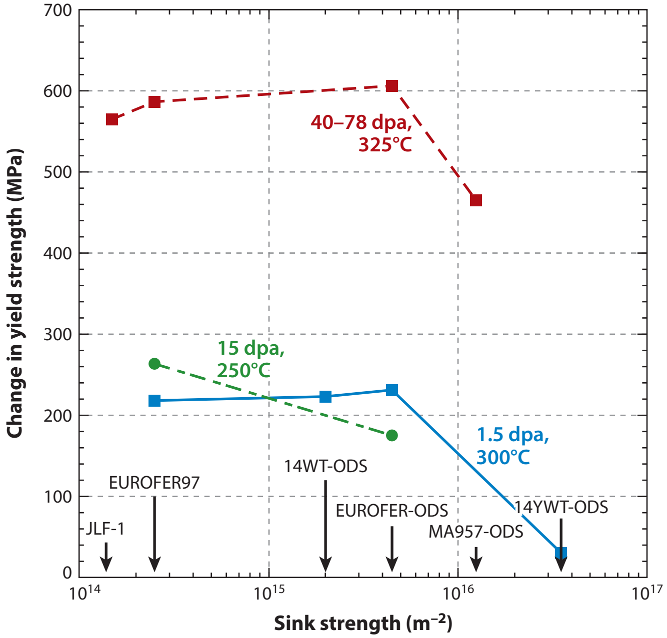

Figure 10

Effect of initial sink strength on the radiation hardening of steels following fission neutron irradiation near 300°C to damage levels of 1.5 to 78 displacements per atom (dpa). Materials include conventionally fabricated low-activation ferritic/martensitic steels (the Japanese low-activation ferritic JLF-1 and EUROFER) and several oxide dispersion–strengthened (ODS) steels fabricated by using powder metallurgy processes.

in several grades of ODS steels provide sink strengths near or greater than $10^{16}/m^2$ (**Figure 10**), although this effectiveness still remains to be proven up to high doses. High sink strengths can also be achieved via nanoscale films (which have a high surface-to-volume ratio) or via closely spaced grain boundaries or multilayered structures (124–128).

An important point from rate theory modeling analyses (55, 106, 123) is that the ratio of the total sink strength to the dislocation sink strength (rather than simply the total sink strength) has a major influence on radiation defect accumulation. In particular, cavity swelling is maximized when the ratio of the dislocation sink strength to the cavity sink strength is near unity (16, 55); under this scenario, efficient (biased) partitioning of interstitials to dislocations is facilitated, thereby resulting in maximum vacancy supersaturation.

One proposed strategy for radiation-resistant materials is based on nucleation of a high concentration of small He bubbles, which presumably promotes point defect recombination via their high sink strength, simultaneously delaying the conversion of bubbles to bias-driven (rapid) growth by diluting the He over numerous cavity sites (111, 123, 129, 130). This concept is appealing for moderate radiation environments, but for the extreme dose and He generation conditions in fusion reactors (**Figure 3**), it may not provide sufficient radiation resistance. To achieve a cavity sink strength of $\sim 10^{16}/m^2$ (Equation 2 and **Figures 10** and **11**) for overall radiation resistance while simultaneously keeping volumetric swelling to less than 5%, an extremely high density ($>5 \times 10^{23}/m^3$) of small cavities is required, as shown in **Figure 12**. Several of the highest-density experimentally observed cavity parameters for neutron- and ion-irradiated metals (131–133) are plotted in **Figure 12**. Even for the relatively high He/dpa conditions in

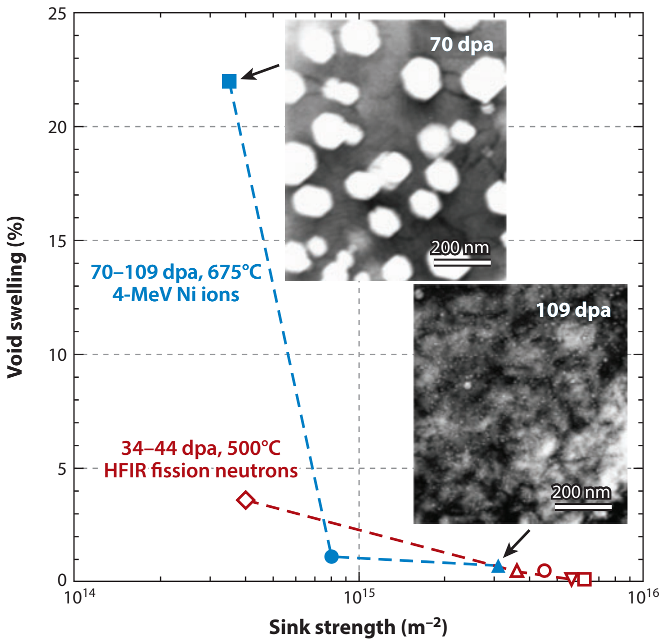

Figure 11

Effect of sink strength on the volumetric void swelling of ion-irradiated (4-MeV Ni and 200–400-keV He) and fission neutron–irradiated Fe-Cr-Ni austenitic alloys. Symbols denote the following: blue square, P7 pure type 316 stainless steel (Reference 118); blue circle, B11 cold-worked Ti- and P-modified Fe-14Cr-15Ni austenitic steel (Reference 119); blue triangle, B12 cold-worked Ti-, P-, and Si-modified Fe-14Cr-15Ni austenitic steel (Reference 119); red diamond, N lot type 316 stainless steel (Reference 121); red triangle, A3 prime candidate alloy (PCA) Ti-modified type 316 stainless steel (Reference 121); red circle, solution-annealed Japanese PCA (JPCA) Ti-modified type 316 stainless steel (Reference 120); red inverted triangle, cold-worked PCA Ti-modified type 316 stainless steel (Reference 121); red square, cold-worked JPCA Ti-modified type 316 stainless steel (Reference 120).

these experiments compared with fusion-relevant conditions, ultrahigh cavity densities were not achieved; the maximum cavity densities for neutron irradiation conditions obtained to date are 3 to 10 times lower than needed to achieve the desired ultrahigh sink strengths from cavities alone.

The high-sink-strength mechanism can be combined with the radiation-resistant matrix phase mechanism (Section 3.1) to engineer very potent radiation resistance. Such a combined approach is the basis for the apparent superior performance of ODS ferritic steels (e.g., **Figure 10** and References 132, 134, and 135) that combine a radiation-resistant ferrite matrix with the high sink density of nanoscale dispersoids.

4. ENGINEERING DESIGN OF ADVANCED MATERIALS

4.1. Computational Thermodynamics

Remarkable progress in density functional theory models now allows numerous atomistic properties to be accurately calculated in materials (84). Similarly, the advent of a suite of computational thermodynamic software tools has led to a marked acceleration in the design of new high-performance materials over the past 15 years (136–140). These computational thermodynamics studies have concluded that many current commercial alloys are far from optimized,

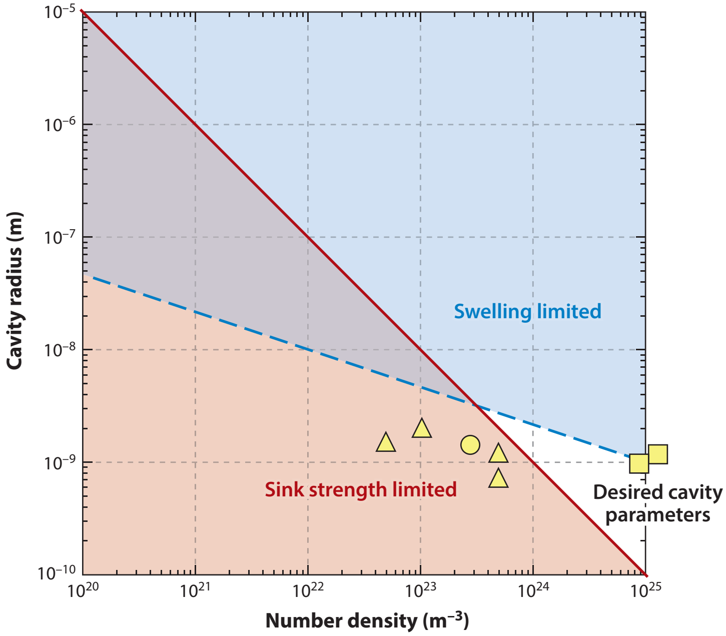

Figure 12

Relationship between cavity size and density for simultaneously achieving a cavity sink strength of $>10^{16}/\mathrm{m}^2$ (**Equation 2**) and a volumetric swelling $4\pi r_C{}^3 N_C/3$ of less than 5%. The data points show experimentally observed cavity parameters for neutron-irradiated steels [*circle* and *triangles* (from References 131 and 132)] and for He ion–implanted metals [*squares* (from Reference 133)].

with allowable solute compositions and heat treatments that in some cases could give rise to undesired phases (139, 141). If one takes into consideration the principles for designing radiation-resistant materials discussed in Section 3, ferritic/martensitic alloys containing a high density of uniformly dispersed, highly stable precipitates or dispersoids are of considerable interest. By using thermomechanical treatments along with targeted modification in the composition of minor elements, precipitate densities that are up to a factor of ~1,000 higher than those of conventional ferritic/martensitic steels have been designed and fabricated; the tensile strength concomitantly increases by ~50%, with no appreciable reduction in ductility or fracture toughness compared with conventional steels (140, 142, 143). The calculated defect sink strengths for these new steels are on the order of a few times $10^{15}/\mathrm{m}^2$, which is near the lower bound of the sink strength required to provide superior radiation resistance (see Section 3.3; **Figures 10** and **11**). Some scoping irradiation experiments are currently in progress to assess the radiation performance of these new ferritic/martensitic steels (140). In the future, further optimization to include tailored resistance to specific phenomena such as design-specific creep-fatigue processes may be envisioned.

4.2. Advanced Manufacturing

In parallel with the advances in designing new materials with computational thermodynamics tools, rapid progress has recently been achieved in a host of new advanced manufacturing processes. Of particular interest are additive manufacturing techniques (144, 145), such as electron beam melting that enables precision manufacturing of complex geometries a few atomic planes at a time, and ultrasonic manufacturing that, for example, facilitates precise insertion of embedded sensors. Advantages of additive manufacturing over conventional processing include the potential for atomic-scale materials engineering/fabrication, much less waste material (particularly important for rare or expensive materials), rapid component prototyping and optimization (due in part to direct utilization of CAD drawings), and the possibility of fabricating components that would be impossible to produce by conventional manufacturing techniques. These additive manufacturing techniques could potentially be used to create unique engineering architectures (e.g., enhanced heat transfer swirl tubes) that would be beneficial for fusion energy applications. However, there may be a potential trade-off between the improved ability to manufacture complex geometries and the reduced performance of the base material because the current advanced manufacturing techniques are not easily amenable to the postfabrication thermomechanical treatments that are conventionally required to produce optimum materials properties and radiation resistance. Further research is needed to determine the base materials properties of components fabricated by using additive manufacturing techniques and subsequently to investigate modifications of additive manufacturing processing conditions that might lead to enhanced properties (including those specifically tailored for radiation resistance).

4.3. Environmental and Safety Considerations

A key objective for fusion is to reliably and economically generate power without the need for public evacuation under design-basis-accident scenarios. The D-T fusion reaction does not directly create radiological products (if higher-order cross-product reactions are ignored). However, transmutation reactions by energetic fusion neutrons (Equation 1) can create radioactive isotopes in the materials surrounding the plasma chamber. Therefore, careful selection of materials in the fusion chamber is required to simultaneously minimize long-lived radioactive species (for waste recycling and disposal) and short-term decay heat and production of volatile radioactive or hazardous species (for public and worker safety) (18, 21). Dispersal of radiological species is a potential safety concern under transient situations such as loss-of-coolant accidents and station blackout conditions, in which residual afterheat from neutron-induced transmutation decay chain isotopes can cause gradual heating of the fusion reactor chamber (even when the fusion reaction is stopped) if flowing coolant is not available. For example, safety calculations of the decay heat and potential volatization of radiological species stemming from transmutation of Mn in a loss-of-coolant accident (21) led to the abandonment of fusion research on Mn-stabilized austenitic steels (where Mn replaced Ni to reduce long-lived radioactivity), even though these steels exhibited low, long-term (>100-year) radioactivity.

Several studies observed enhanced H isotope trapping in materials following irradiation (146–149). This enhanced trapping raises safety concerns because large amounts of tritium from the D-T fuel could be trapped in plasma-facing or structural components of a fusion reactor and subsequently released during a loss-of-cooling accident. H trapping appears to be particularly pronounced when cavities are present (10, 147) but appears to be relatively modest at lower irradiation temperatures, at which other microstructural configurations predominate (see **Figure 4** for an overview of temperature-dependent microstructures). Therefore, one should perform H-trapping evaluations on materials that have been irradiated at reactor-relevant temperatures, keeping in mind that the high transmutant He generation from energetic D-T fusion neutrons is an additional stimulant for cavity formation (46, 59). Recent simulation studies found that H is strongly trapped near the surfaces of cavities in Fe and W (150, 151). If high cavity sink strengths are present (see **Figure 12**), tritium sequestration issues could become a controlling consideration. For example, if one assumed monolayer coverage on cavities in the ~1-cm-thick W tiles in the plasma-facing regions in a fusion reactor [an ~850-m^2 surface area in ITER (152)], the product of the cavity density and radius squared would need to be $N_C r_C^2 < 10^5$/m to stay below the ~740-g ITER site limit for tritium. This tritium-trapping limit would place severe constraints on the allowable cavity sizes and densities in the W armor (e.g., $N_C < 10^{23}/\mathrm{m}^3$ for an average cavity radius of 1 nm), which might require frequent replacement or maintenance of the plasma-facing armor to keep the tritium inventory at an acceptable level. Even more restrictive cavity parameters would apply for first-wall and blanket structures in a future DEMO fusion reactor due to their larger volume. As noted elsewhere (10, 141, 148), further research is needed to understand and quantify tritium-trapping mechanisms in irradiated materials. However, using high cavity sink strengths as a strategy for radiation resistance may be problematic in fusion reactors due to tritium-trapping considerations.

5. CONCLUSIONS

The materials to be deployed in fusion reactors must satisfy stringent environmental and safety requirements in addition to maintaining high performance in the harsh D-T neutron environment. On the basis of these considerations, the most promising strategy for designing structural materials for fusion energy applications is to use either high noncavity sink strengths such as precipitates or dispersoids in BCC materials (e.g., thermomechanically treated or ODS RAFM steel) or materials in which vacancies are immobile at the design operating temperatures (e.g., SiC/SiC composites). Similar principles may be valuable for the selection of key materials systems in advanced (Generation IV) fission reactors. The potential confluence of accurate multiscale models and emerging advanced manufacturing techniques offers an attractive prospect for the future design of complex components.

FUTURE ISSUES

1. An appropriate high-flux fusion neutron irradiation facility is needed to validate radiation-resistant materials concepts, quantification of tritium-trapping issues in materials, exploration of basic maintenance and repair issues of irradiated materials, and development of an irradiated materials engineering database for fusion reactor design and licensing.
2. The engineering design rules for low-ductility materials are incomplete (157). ITER developed modified design rules to use austenitic stainless steel with low uniform elongation (due to radiation hardening). These design rules should be further extended to include W, SiC, and other low-toughness steels.
3. Engineering and/or materials science solutions to resolve the low irradiation dose lifetimes of many of the current candidate functional materials systems for fusion should be developed.

DISCLOSURE STATEMENT

The authors are not aware of any affiliations, memberships, funding, or financial holdings that might be perceived as affecting the objectivity of this review.

ACKNOWLEDGMENTS

This work was supported by the Office of Fusion Energy Sciences and the Office of Nuclear Energy, US Department of Energy, under contract DE-AC05-00OR22725 with UT-Battelle, LLC. We thank M. Sawan, R. Feder, and M. Youssef for the neutronic results summarized in

Figure 1; Y. Osetsky for the molecular dynamics simulations shown in **Figure 2**; and J.T. Busby and K.J. Leonard for providing two of the images in **Figure 4**.

LITERATURE CITED

1. Chu S, Majumdar A. 2012. Opportunities and challenges for a sustainable energy future. *Nature* 488:294–303
2. Zinkle SJ, Was GS. 2013. Materials challenges in nuclear energy. *Acta Mater.* 61:735–58
3. Post RF, Ribe FL. 1974. Fusion reactors as future energy sources. *Science* 186:397–407
4. Gordinier MR, Davis JW, Scott FR, Schultz KR. 2003. Nuclear fusion power. In *Encyclopedia of Physical Science and Technology*, Vol. 10, ed. RA Meyers, pp. 671–99. New York: Academic. 3rd ed.
5. Lehnert B. 2013. Half a century of fusion research towards ITER. *Phys. Scr.* 87:018201
6. Boozer AH. 2004. Physics of magnetically confined plasmas. *Rev. Mod. Phys.* 76:1071–141
7. Moses EI, Boyd RN, Remington BA, Keane CJ, Al-Ayat R. 2009. The National Ignition Facility: ushering in a new age for high energy density science. *Phys. Plasmas* 16:041006
8. Ihli T, Basu TK, Giancarli LM, Konishi S, Malang S, et al. 2008. Review of blanket designs for advanced fusion reactors. *Fusion Eng. Des.* 83:912–19
9. Giancarli LM, Abdou M, Campbell DJ, Chuyanov VA, Ahn MY, et al. 2012. Overview of the ITER TBM Program. *Fusion Eng. Des.* 87:395–402
10. Zinkle SJ, Möslang A, Muroga T, Tanigawa H. 2013. Multimodal options for materials research to advance the basis for fusion energy in the ITER era. *Nucl. Fusion* 53:104024
11. Bühler L. 1995. The influence of small cracks in insulating coatings on the flow structure and pressure drop in MHD channel flows. *Fusion Eng. Des.* 27:650–58
12. Moreau R, Brechet Y, Maniguet L. 2011. Eurofer corrosion by the flow of the eutectic alloy Pb–Li in the presence of a strong magnetic field. *Fusion Eng. Des.* 86:106–20
13. Roux N, Hollenberg G, Johnson C, Noda K, Verrall R. 1995. Summary of experimental results for ceramic breeder materials. *Fusion Eng. Des.* 27:154–66
14. Bloom EE. 1998. The challenge of developing structural materials for fusion power systems. *J. Nucl. Mater.* 258–263:7–17
15. Bloom EE, Zinkle SJ, Wiffen FW. 2004. Materials to deliver the promise of fusion power—progress and challenges. *J. Nucl. Mater.* 329–333:12–19
16. Odette GR, Alinger MJ, Wirth BD. 2008. Recent developments in irradiation-resistant steels. *Annu. Rev. Mater. Res.* 38:471–503
17. Zinkle SJ, Busby JT. 2009. Structural materials for fission and fusion energy. *Mater. Today* 12:12–19
18. Holdren JP, Berwald DH, Budnitz RJ, Crocker JG, Delene JG, et al. 1988. Exploring the competitive potential of magnetic fusion energy—the interaction of economics with safety and environmental characteristics. *Fusion Technol.* 13:7–56
19. Holdren JP. 1978. Fusion energy in context: its fitness for the long term. *Science* 200:168–80
20. Bloom EE, Conn RW, Davis JW, Gold RE, Little R, et al. 1984. Low activation materials for fusion applications. *J. Nucl. Mater.* 122–123:17–26
21. Piet SJ, Cheng ET, Fetter S, Herring JS. 1991. Initial integration of accident safety, waste management, recycling, effluent, and maintenance considerations for low-activation materials. *Fusion Technol.* 19:146–61
22. Cheng ET. 1998. Concentration limits of natural elements in low activation fusion materials. *J. Nucl. Mater.* 258–263:1767–72
23. Klueh RL. 2004. Reduced-activation bainitic and martensitic steels for nuclear fusion applications. *Curr. Opin. Solid State Mater. Sci.* 8:239–50
24. Tanigawa H, Shiba K, Möslang A, Stoller RE, Lindau R, et al. 2011. Status and key issues of reduced activation ferritic/martensitic steels as the structural material for a DEMO blanket. *J. Nucl. Mater.* 417:9–15
25. Ukai S, Fujiwara M. 2002. Perspective of ODS alloys application in nuclear environments. *J. Nucl. Mater.* 307–311:749–57

26. Klueh RL, Shingledecker JP, Swindeman RW, Hoelzer DT. 2005. Oxide dispersion–strengthened steels: a comparison of some commercial and experimental alloys. *J. Nucl. Mater.* 341:103–14
27. Lindau R, Möslang A, Rieth M, Klimankou M, Materna-Morris E, et al. 2005. Present development status of EUROFER and ODS for application in blanket concepts. *Fusion Eng. Des.* 75–79:989–96
28. Zinkle SJ. 2005. Advanced materials for fusion technology. *Fusion Eng. Des.* 74:31–40
29. Smith DL, Billone MC, Majumdar S, Mattas RF, Sze D-K. 1998. Materials integration issues for high-performance fusion power systems. *J. Nucl. Mater.* 258–263:65–73
30. Zinkle SJ, Matsui H, Smith DL, Rowcliffe AF, van Osch E, et al. 1998. Research and development on vanadium alloys for fusion applications. *J. Nucl. Mater.* 258–263:205–14
31. Muroga T, Chen JM, Chernov VM, Fukumoto K, Hoelzer DT, et al. 2007. Review of advances in development of vanadium alloys and MHD insulator coatings. *J. Nucl. Mater.* 367–370:780–87
32. Snead LL, Nozawa T, Ferraris M, Katoh Y, Shinavski R, Sawan M. 2011. Silicon carbide composites as fusion power reactor structural materials. *J. Nucl. Mater.* 417:330–39
33. Pitts RA, Carpentier S, Escourbiac F, Hirai T, Komarov V, et al. 2011. Physics basis and design of the ITER plasma-facing components. *J. Nucl. Mater.* 415:S957–64
34. Wirth BD, Nordlund K, Whyte DG, Xu D. 2011. Fusion materials modeling: challenges and opportunities. *MRS Bull.* 36:216–22
35. Linke J. 2012. High heat flux performance of plasma facing materials and components under service conditions in future fusion reactors. *Fusion Sci. Technol.* 61:246–55
36. Bolt H, Barabash VR, Federici G, Linke J, Loarte A, et al. 2002. Plasma facing and high heat flux materials—needs for ITER and beyond. *J. Nucl. Mater.* 307–311:43–52
37. Neu R. 2011. Preparing the scientific basis for an all metal ITER. *Plasma Phys. Control. Fusion* 53:124040
38. Romanelli F. 2013. Overview of the JET results with the ITER-like wall. *Nucl. Fusion* 53:104002
39. Barabash V, Federici G, Linke J, Wu CH. 2003. Material/plasma surface interaction issues following neutron damage. *J. Nucl. Mater.* 313:42–51
40. Nygren RE, Raffray R, Whyte D, Ulrickson MA, Baldwin M, Snead LL. 2011. Making tungsten work. *J. Nucl. Mater.* 417:451–56
41. Rieth M, Dudarev SL, Gonzalez de Vicente SM, Aktaa J, Ahlgren R, et al. 2013. Recent progress in research on tungsten materials for nuclear fusion applications in Europe. *J. Nucl. Mater.* 432:482–500
42. Greenwood LR, Garner FA. 1994. Transmutation of Mo, Re, W, Hf and V in various irradiation test facilities and STARFIRE. *J. Nucl. Mater.* 212–215:635–39
43. Dai Y, Odette GR, Yamamoto T. 2012. The effects of helium in irradiated structural alloys. See Ref. 153, pp. 141–93
44. Trinkaus H, Singh BN. 2003. Helium accumulation in metals during irradiation—where do we stand? *J. Nucl. Mater.* 323:229–42
45. Zinkle SJ, Möslang A. 2013. Evaluation of irradiation facility options for fusion materials research and development. *Fusion Eng. Des.* 88:472–82
46. Zinkle SJ. 2012. Radiation-induced effects on microstructure. See Ref. 153, pp. 65–98
47. Schilling W, Ehrhart P, Sonnenberg K. 1975. Interpretation of defect reactions in irradiated metals by the one interstitial model. In *Fundamental Aspects of Radiation Damage in Metals*, Vol. I, Rep. CONF-751006-P1, ed. MT Robinson, FW Young Jr, pp. 470–92. Springfield, VA: Natl. Tech. Inf. Serv.
48. Schilling W, Sonnenberg K. 1973. Recovery of irradiated and quenched metals. *J. Phys. F* 3:322–50
49. Weber WJ. 2000. Models and mechanisms of irradiation-induced amorphization in ceramics. *Nucl. Instrum. Methods Phys. Res. B* 166:98–106
50. Ullmaier H, Carsughi F. 1995. Radiation damage problems in high power spallation neutron sources. *Nucl. Instrum. Methods Phys. Res. B* 101:406–21
51. Zinkle SJ. 2005. Fusion materials science: overview of challenges and recent progress. *Phys. Plasmas* 12:058101
52. Odette GR, Yamamoto T, Rathbun HJ, He MY, Hribernik ML, Rensman JW. 2003. Cleavage fracture and irradiation embrittlement of fusion reactor alloys: mechanisms, multiscale models, toughness measurements and implications to structural integrity assessment. *J. Nucl. Mater.* 323:313–40
53. Schroeder H, Ullmaier H. 1991. Helium and hydrogen effects on the embrittlement of iron- and nickel-based alloys. *J. Nucl. Mater.* 179–181:118–24

54. Garner FA, Toloczko MB, Sencer BH. 2000. Comparison of swelling and irradiation creep behavior of fcc-austenitic and bcc-ferritic/martensitic alloys at high neutron exposure. *J. Nucl. Mater.* 276:123–42
55. Mansur LK. 1994. Theory and experimental background on dimensional changes in irradiated alloys. *J. Nucl. Mater.* 216:97–123
56. Maziasz PJ. 1989. Formation and stability of radiation-induced phases in neutron-irradiated austenitic and ferritic steels. *J. Nucl. Mater.* 169:95–115
57. Okamoto PR, Rehn LE. 1979. Radiation-induced segregation in binary and ternary alloys. *J. Nucl. Mater.* 83:2–23
58. Mansur LK, Lee EH, Maziasz PJ, Rowcliffe AF. 1986. Control of helium effects in irradiated materials based on theory and experiment. *J. Nucl. Mater.* 141–143:633–46
59. Stoller RE. 1990. The influence of helium on microstructural evolution: implications for DT fusion reactors. *J. Nucl. Mater.* 174:289–310
60. Wakai E, Kikuchi K, Yamamoto S, Aruga T, Ando M, et al. 2002. Swelling behavior of F82H steel irradiated by triple/dual ion beams. *J. Nucl. Mater.* 318:267–73
61. Zinkle SJ, Snead LL. 1996. Influence of irradiation spectrum and implanted ions on the amorphization of ceramics. *Nucl. Instrum. Methods Phys. Res. B* 116:92–101
62. Trachenko K. 2004. Understanding resistance to amorphization by radiation damage. *J. Phys. Condens. Matter* 16:R1491–515
63. IAEA. 2013. *Operating Experience with Nuclear Power Stations in Member States in 2012*. Vienna: IAEA
64. Yamamoto S, Shikama T, Belyakov V, Farnum E, Hodgson E, et al. 2000. Impact of irradiation effects on design solutions for ITER diagnostics. *J. Nucl. Mater.* 283–287:60–69
65. Vayakis G, Hodgson ER, Voitsenya V, Walker CI. 2008. Generic diagnostic issues for a burning plasma experiment. *Fusion Sci. Technol.* 53:699–750
66. Zinkle SJ, Hodgson ER. 1992. Radiation-induced changes in the physical properties of ceramic materials. *J. Nucl. Mater.* 191–194:58–66
67. Itoh N, Stoneham AM. 2001. *Materials Modification by Electronic Excitation*. Cambridge, UK: Cambridge Univ. Press. 536 pp.
68. Nishitani T, Ishitsuka E, Kakuta T, Sagawa H, Noda K, et al. 1998. Japanese contribution to ITER task of irradiation tests on diagnostics components. *Fusion Eng. Des.* 42:443–48
69. Snead LL, Leonard KJ, Jellison GE, Sawan M, Lehecka T. 2009. Irradiation effects on dielectric mirrors for fusion power reactor application. *Fusion Sci. Technol.* 56:1069–77
70. Brichard B, Borgermans P, Fernandez AF, Lammens K, Decreton M. 2001. Radiation effect in silica optical fiber exposed to intense mixed neutron-gamma radiation field. *IEEE Trans. Nucl. Sci.* 48:2069–73
71. Sickafus KE, Grimes RW, Valdez JA, Cleave A, Tang M, et al. 2007. Radiation-induced amorphization resistance and radiation tolerance in structurally related oxides. *Nat. Mater.* 6:217–23
72. Stiegler JO, Bloom EE. 1971. The effect of thermo-mechanical treatments on void formation in irradiated stainless steel. *J. Nucl. Mater.* 41:341–44
73. Brager HR, Garner FA, Gilbert ER, Flinn JE, Wolfer WG. 1977. Stress-affected microstructural development and the creep-swelling interrelationship. See Ref. 154, pp. 727–55
74. Zinkle SJ, Maziasz PJ, Stoller RE. 1993. Dose dependence of the microstructural evolution in neutron-irradiated austenitic stainless steel. *J. Nucl. Mater.* 206:266–86
75. Bates JF, Johnston WG. 1977. Effects of alloy composition on void swelling. See Ref. 154, pp. 625–44
76. Venker H, Giesecke P, Ehrlich K. 1977. The influence of fast diffusing substitutional elements on the swelling behaviour of Ni- and Cu-alloys. See Ref. 154, pp. 415–20
77. Bloom EE, Stiegler JO. 1970. A comparison of irradiation-induced swelling and void formation in two austenitic stainless steels. *J. Nucl. Mater.* 35:244–46
78. Maziasz PJ. 1984. Swelling and swelling resistance possibilities of austenitic stainless steels in fusion reactors. *J. Nucl. Mater.* 122–123:472–86
79. Klabunde CE, Coltman RR Jr. 1982. Fission neutron damage rates and efficiencies in several metals. *J. Nucl. Mater.* 108–109:183–93
80. Wallner G, Anand MS, Greenwood LR, Kirk MA, Mansel W, Waschkowski W. 1988. Defect production rates in metals by reactor neutron irradiation at 4.6 K. *J. Nucl. Mater.* 152:146–53

81. English CA. 1982. Low-dose neutron irradiation damage in FCC and BCC metals. *J. Nucl. Mater.* 108–109:104–23
82. Jenkins ML, Kirk MA, Phythian WJ. 1993. Experimental studies of cascade phenomena in metals. *J. Nucl. Mater.* 205:16–30
83. Bacon DJ, Gao F, Osetsky YN. 2000. The primary damage state in fcc, bcc and hcp metals as seen in molecular dynamics simulations. *J. Nucl. Mater.* 276:1–12
84. Dudarev SL. 2013. Density functional theory models for radiation damage. *Annu. Rev. Mater. Res.* 43:35–61
85. Sniegowski JJ, Wolfer WG. 1984. On the physical basis for the swelling resistance of ferritic steels. *Proc. Topical Conference on Ferritic Alloys for Use in Nuclear Energy Technologies*, ed. JW Davis, DJ Michel, pp. 579–86. New York: TMS/AIME
86. Nakajima H, Yoshida S, Kohno Y, Matsui H. 1992. Effect of solute addition on swelling of vanadium after FFTF irradiation. *J. Nucl. Mater.* 191–194:952–55
87. Abe Y, Matsui H. 2007. Effects of undersized Fe atoms on the stability of interstitials near a dislocation core in V studied by molecular dynamics simulation. *J. Comp. Aided Mater. Des.* 14:121–27
88. Yeh JW, Chen SK, Lin SJ, Gan JY, Chin TS, et al. 2004. Nanostructured high-entropy alloys with multiple principal elements: novel alloy design concepts and outcomes. *Adv. Eng. Mater.* 6:299–303
89. Kiran Kumar NAP, Leonard KJ, Bei H, Zhang Y, Zinkle SJ. 2014. Microstructural stability and mechanical behavior of FeMnNiCr high entropy alloy under ion irradiation. *J. Nucl. Mater.* Submitted
90. Sickafus KE, Minervini L, Grimes RW, Valdez JA, Ishimaru M, et al. 2000. Radiation tolerance of complex oxides. *Science* 289:748–51
91. Inoue A. 2000. Stabilization of metallic supercooled liquid and bulk amorphous alloys. *Acta Mater.* 48:279–306
92. Primak W. 1958. Fast-neutron-induced changes in quartz and vitreous silica. *Phys. Rev.* 110:1240–54
93. Weber WJ, Ewing RC, Angell CA, Arnold GW, Cormack AN, et al. 1997. Radiation effects in glasses used for immobilization of high level waste and plutonium disposition. *J. Mater. Res.* 12:1946–75
94. Nakagawa M, Mansel W, Boning K, Rosner P, Vogl G. 1979. Spontaneous recombination volumes of Frenkel defects in neutron-irradiated non-FCC metals. *Phys. Rev. B* 19:742–48
95. Birtcher RC, Blewitt TH. 1981. Damage saturation effects on volume and resistivity changes induced by fission-fragment irradiation of copper. *J. Nucl. Mater.* 98:63–70
96. Birtcher RC, Blewitt TH. 1988. Cascade damage in nickel—production, saturation and recovery. *J. Nucl. Mater.* 152:204–11
97. Trinkaus H. 1997. Ion beam induced amorphization of crystalline solids: mechanisms and modeling. *Mater. Sci. Forum* 248–249:3–12
98. Keilholtz GW, Lee JE Jr, Moore RE. 1966. Irradiation damage to sintered beryllium oxide as a function of fast-neutron dose and flux at 110, 650, and 1100°C. *Nucl. Sci. Eng.* 26:329–38
99. Wilks RS. 1968. Neutron-induced damage in BeO, Al_2O_3 and MgO—a review. *J. Nucl. Mater.* 26:137–73
100. Katoh Y, Snead LL. 2009. Operating temperature window for SiC ceramics and composites for fusion energy applications. *Fusion Sci. Technol.* 56:1045–52
101. Keilholtz GW, Moore RE, Robertson HE. 1973. Fast-neutron damage to polycrystalline alumina at temperatures from 60 to 1230°C. *Nucl. Technol.* 17:234–46
102. Katoh Y, Nozawa T, Snead LL, Ozawa K, Tanigawa H. 2011. Stability of SiC and its composites at high neutron fluence. *J. Nucl. Mater.* 417:400–5
103. Snead LL, Zinkle SJ, Hay JC, Osborne MC. 1998. Amorphization of SiC under ion and neutron irradiation. *Nucl. Instrum. Methods Phys. Res. B* 141:123–32
104. Latham CD, Heggie MI, Alatalo M, Oberg S, Briddon PR. 2013. The contribution made by lattice vacancies to the Wigner effect in radiation-damaged graphite. *J. Phys. Condens. Matter* 25:135403
105. Snead LL, Katoh Y, Connery S. 2007. Swelling of SiC at intermediate and high irradiation temperatures. *J. Nucl. Mater.* 367–370:677–84
106. Brailsford AD, Bullough R. 1972. The rate theory of swelling due to void growth in irradiated metals. *J. Nucl. Mater.* 44:121–35
107. Johnson RA, Lam NQ. 1976. Solute segregation in metals under irradiation. *Phys. Rev. B* 13:4364–75

108. Adda Y. 1972. Report on the CEA program of investigations of radiation-induced cavities in metals: presentation of some results. In *Radiation-Induced Voids in Metals*, ed. JW Corbett, LC Ianniello, pp. 31–81. Springfield, VA: Natl. Tech. Inf. Serv.
109. Brager HR. 1975. The effects of cold working and pre-irradiation heat treatment on void formation in neutron-irradiated type 316 stainless steel. *J. Nucl. Mater.* 57:103–18
110. Williams TM, Titchmarsh JM, Arkell DR. 1982. Void-swelling and precipitation in a neutron-irradiated, niobium-stabilised austenitic stainless steel. *J. Nucl. Mater.* 107:222–44
111. Lee EH, Mansur LK. 1992. Relationships between phase stability and void swelling in Fe-Cr-Ni alloys during irradiation. *Metall. Trans. A* 23:1977–86
112. McClintock DA, Sokolov MA, Hoelzer DT, Nanstad RK. 2009. Mechanical properties of irradiated ODS-EUROFER and nanocluster strengthened 14YWT. *J. Nucl. Mater.* 392:353–59
113. Möslang A, Adelhelm C, Heidinger R. 2008. Innovative materials for energy technology. *Int. J. Mater. Res.* 99:1045–54
114. Henry J, Averty X, Alamo A. 2011. Tensile and impact properties of 9Cr tempered martensitic steels and ODS-FeCr alloys irradiated in a fast reactor at 325°C up to 78 dpa. *J. Nucl. Mater.* 417:99–103
115. Maziasz PJ. 1980. Helium trapping and Ti-rich MC particles in neutron-irradiated type 316 + Ti stainless steels. *Scr. Metall.* 14:1251–56
116. Kesternich W. 1985. A possible solution of the problem of helium embrittlement. *J. Nucl. Mater.* 127:153–60
117. Schroeder H. 1988. High temperature helium embrittlement in austenitic stainless steels—correlations between microstructure and mechanical properties. *J. Nucl. Mater.* 155–157:1032–37
118. Packan NH, Farrell K. 1979. Simulation of first wall damage: effects of the method of gas implantation. *J. Nucl. Mater.* 85–86:677–81
119. Lee EH, Packan NH. 1989. Swelling suppression in phosphorus-modified Fe-Cr-Ni alloys during neutron irradiation. *Int. Symp. Eff. Radiat. Mater.*, 14th, ed. NH Packan, RE Stoller, AS Kumar, pp. 133–46. Philadelphia: Am. Soc. Test. Mater.
120. Tanaka MP, Hamada S, Hishinuma A, Maziasz PJ. 1988. Microstructural development of austenitic stainless steels irradiated in HFIR. *J. Nucl. Mater.* 155:801–5
121. Maziasz PJ. 1993. Void swelling resistance of phosphorus-modified austenitic stainless steels during HFIR irradiation at 300–500°C to 57 dpa. *J. Nucl. Mater.* 200:90–107
122. Kim I-S, Hunn JD, Hashimoto N, Larson DL, Maziasz PJ, et al. 2000. Defect and void evolution in oxide dispersion strengthened ferritic steels under 3.2 MeV Fe^{+} ion irradiation with simultaneous helium injection. *J. Nucl. Mater.* 280:264–74
123. Odette GR, Hoelzer DT. 2010. Irradiation-tolerant nanostructured ferritic alloys: transforming helium from a liability to an asset. *JOM* 62:84–92
124. Lam NQ, Rothman SJ, Sizmann R. 1974. Steady-state point-defect diffusion profiles in solids during irradiation. *Radiat. Effects* 23:53–59
125. Singh BN, Foreman AJE. 1974. Calculated grain size-dependent vacancy supersaturation and its effect on void formation. *Philos. Mag.* 29:847–57
126. Bullough R, Hayns MR, Wood MH. 1980. Sink strengths for thin film surfaces and grain boundaries. *J. Nucl. Mater.* 90:44–59
127. Zinkle SJ. 1994. Microstructure of ion irradiated ceramic insulators. *Nucl. Instrum. Meth. Phys. Res. B* 91:234–46
128. Demkowicz MJ, Bellon P, Wirth BD. 2010. Atomic-scale design of radiation-tolerant nanocomposites. *MRS Bull.* 35:992–98
129. Lee EH, Mansur LK. 1990. Unified theoretical analysis of experimental swelling data for irradiated austenitic and ferritic martensitic alloys. *Metall. Trans. A* 21:1021–35
130. Mansur LK, Lee EH. 1991. Theoretical basis for unified analysis of experimental data and design of swelling-resistant alloys. *J. Nucl. Mater.* 179–181:105–10
131. Edwards DJ, Garner FA, Bruemmer SM, Efsing P. 2009. Nano-cavities observed in a 316SS PWR flux thimble tube irradiated to 33 and 70 dpa. *J. Nucl. Mater.* 384:249–55
132. Odette GR, Miao P, Edwards DJ, Yamamoto T, Kurtz RJ, Tanigawa H. 2011. Helium transport, fate and management in nanostructured ferritic alloys: in situ helium implanter studies. *J. Nucl. Mater.* 417:1001–4

133. Ghoniem NM, Walgraef D, Zinkle SJ. 2001. Theory and experiment of nanostructure self-organization in irradiated materials. *J. Comp. Aided Mater. Des.* 8:1–38
134. Toloczko MB, Garner FA, Maloy SA. 2012. Irradiation creep and density changes observed in MA957 pressurized tubes irradiated to doses of 40–110 dpa at 400–750 degrees C in FFTF. *J. Nucl. Mater.* 428:170–75
135. Certain A, Kuchibhatla S, Shutthanandan V, Hoelzer DT, Allen TR. 2013. Radiation stability of nanoclusters in nano-structured oxide dispersion strengthened (ODS) steels. *J. Nucl. Mater.* 434:311–21
136. Olson GB. 1997. Computational design of hierarchically structured materials. *Science* 277:1237–42
137. Andersson JO, Helander T, Hoglund LH, Shi PF, Sundman B. 2002. THERMO-CALC & DICTRA, computational tools for materials science. *CALPHAD* 26:273–312
138. Curtarolo S, Hart GLW, Nardelli MB, Mingo N, Sanvito S, Levy O. 2013. The high-throughput highway to computational materials design. *Nat. Mater.* 12:191–201
139. Zinkle SJ, Ghoniem NM. 2011. Prospects for accelerated development of high performance structural materials. *J. Nucl. Mater.* 417:2–8
140. Tan L, Yang Y, Busby JT. 2013. Effects of alloying elements and thermomechanical treatment on 9Cr reduced activation ferritic–martensitic (RAFM) steels. *J. Nucl. Mater.* 442(Suppl.):13–17
141. Zinkle SJ. 2013. Challenges in developing materials for fusion technology—past, present, and future. *Fusion Sci. Technol.* 64:65–75
142. Barani AA, Li F, Romano P, Ponge D, Raabe D. 2007. Design of high-strength steels by microalloying and thermomechanical treatment. *Mater. Sci. Eng. A* 463:138–46
143. Klueh RL, Hashimoto N, Maziasz PJ. 2007. New nano-particle-strengthened ferritic/martensitic steels by conventional thermo-mechanical treatment. *J. Nucl. Mater.* 367–370:48–53
144. Kruth J-P, Leu MC, Nakagawa T. 1998. Progress in additive manufacturing and rapid prototyping. *CIRP Ann. Manuf. Technol.* 47:525–40
145. Lipson H. 2012. Frontiers in additive manufacturing: the shape of things to come. *Bridge* 42:5–12
146. Wilson KL, Baskes MI. 1978. Deuterium trapping in irradiated 316 stainless steel. *J. Nucl. Mater.* 76–77:291–97
147. Garner FA, Simonen EP, Oliver BM, Greenwood LR, Grossbeck ML, et al. 2006. Retention of hydrogen in fcc metals irradiated at temperatures leading to high densities of bubbles or voids. *J. Nucl. Mater.* 356:122–35
148. Roth J, Tsitrone E, Loarte A, Loarer T, Counsell G, et al. 2009. Recent analysis of key plasma wall interactions issues for ITER. *J. Nucl. Mater.* 390–391:1–9
149. Alimov VK, Hatano Y, Tyburska-Puschel B, Sugiyama K, Takagi I, et al. 2013. Deuterium retention in tungsten damaged with W ions to various damage levels. *J. Nucl. Mater.* 441:280–85
150. Hayward E, Deo C. 2012. Synergistic effects in hydrogen-helium bubbles. *J. Phys. Condens. Matter* 24:265402
151. Juslin N, Wirth BD. 2013. Molecular dynamics simulation of the effect of sub-surface helium bubbles on hydrogen retention in tungsten. *J. Nucl. Mater.* 438(Suppl.):1221–23
152. Roth J, Tsitrone E, Loarer T, Philipps V, Brezinsek S, et al. 2008. Tritium inventory in ITER plasma-facing materials and tritium removal procedures. *Plasma Phys. Control. Fusion* 50:103001
153. Konings RJM, ed. 2012. *Comprehensive Nuclear Materials*, Vol. 1. Amsterdam: Elsevier
154. Bleiberg ML, Bennett JW. 1977. *Radiation Effects in Breeder Reactor Structural Materials*. New York: TMS/AIME
155. Pakarinen J, Tahtinen S, Singh BN. 2013. A comparative TEM study of in-reactor and post-irradiation tensile tested copper. *J. Nucl. Mater.* 442(Suppl.):821–25
156. Edwards DJ, Singh BN, Bilde-Sorensen JB. 2005. Initiation and propagation of cleared channels in neutron-irradiated pure copper and a precipitation hardened CuCrZr alloy. *J. Nucl. Mater.* 342:164–78
157. Karditsas PJ. 2009. Design issues and implications for structural integrity of fusion power plant components. *Fusion Eng. Des.* 84:2104–8